

SU(4) Kondo effect in double quantum dots with ferromagnetic leadsIreneusz Weymann,^{1,*} Razvan Chirla,^{2,3} Piotr Trocha,¹ and Cătălin Pașcu Moca^{2,4}¹*Faculty of Physics, Adam Mickiewicz University, ul. Umultowska 85, 61-614 Poznań, Poland*²*Department of Physics, University of Oradea, 410087, Oradea, Romania*³*Faculty of Medicine and Pharmacy, Department of Preclinical Sciences, University of Oradea, 410087, Oradea, Romania*⁴*BME-MTA Exotic Quantum Phases Research Group, Budapest University of Technology and Economics, 1521 Budapest, Hungary*

(Received 27 September 2017; revised manuscript received 22 November 2017; published 5 February 2018)

We investigate the spin-resolved transport properties, such as the linear conductance and the tunnel magnetoresistance, of a double quantum dot device attached to ferromagnetic leads and look for signatures of the SU(4) symmetry in the Kondo regime. We show that the transport behavior greatly depends on the magnetic configuration of the device, and the spin-SU(2) as well as the orbital and spin-SU(4) Kondo effects become generally suppressed when the magnetic configuration of the leads varies from the antiparallel to the parallel one. Furthermore, a finite spin polarization of the leads lifts the spin degeneracy and drives the system from the SU(4) to an orbital-SU(2) Kondo state. We analyze in detail the crossover and show that the Kondo temperature between the two fixed points has a nonmonotonic dependence on the degree of spin polarization of the leads. In terms of methods used, we characterize transport by using a combination of analytical and numerical renormalization group approaches.

DOI: [10.1103/PhysRevB.97.085404](https://doi.org/10.1103/PhysRevB.97.085404)**I. INTRODUCTION**

Transport properties of double quantum dots (DQDs)—the simplest realizations of artificial molecules [1]—reveal a plethora of phenomena not present in single quantum dot setups [2–6]. In particular, in the regime of weak coupling between DQD and external electrodes, the interplay of Fermi statistics and charging effects can result in the Pauli spin blockade effect [7–9]. On the other hand, in the strong coupling regime, the many-body electron correlations can result in exotic Kondo effects [10–14], such as the two-stage [14–22] or SU(4) Kondo phenomena [23–32]. In the latter case, the ground state of the system needs to exhibit a fourfold degeneracy, which in the case of DQDs is assured by the spin and orbital degrees of freedom. In fact, the presence of the SU(4) Kondo effect in double quantum dots has recently been confirmed experimentally by A. Keller *et al.* [33]. By applying Zeeman and pseudo-Zeeman fields to break the ground-state degeneracy, it was shown that the measured enhancement of the conductance was indeed due to the formation of the SU(4)-symmetric Kondo state.

The emergence of the Kondo effect can, however, be hindered by the presence of external perturbations [34] or correlations in the leads [35]. In particular, when a quantum dot is attached to ferromagnetic electrodes, the Kondo effect becomes affected due to the development of an exchange field $\Delta\varepsilon_{\text{exch}}$ induced by spin-dependent hybridization [36–40]. Such an exchange field results in a splitting similar to the Zeeman splitting in an external magnetic field [41], still, its sign and magnitude can be tuned by a gate voltage [42–44]. For single-level quantum dots, when the exchange field is getting larger than the corresponding Kondo temperature T_K , the Kondo resonance starts to split. The local density of states exhibits then

only small satellite peaks at energies corresponding to $|\Delta\varepsilon_{\text{exch}}|$ [39–41], instead of a pronounced Abrikosov-Suhl resonance [12,45,46]. For multidot structures, the transport behavior is generally more complex and results from a subtle interplay of the relevant energy scales, with the exchange field playing an important role [47,48].

In this paper, we investigate the linear conductance and the tunnel magnetoresistance in a double quantum dot device and analyze how transport is affected by the presence of ferromagnetic electrodes. We construct the full stability diagram, and identify the regions where the spin-SU(2), orbital-SU(2), and the full SU(4) Kondo states develop. The mere presence of the spin polarization in the leads lifts the spin degeneracy through the exchange field, which, at some particular points in the stability diagram drives the system through a crossover from an SU(4) to an orbital-SU(2) Kondo state [49]. We analyze this crossover in detail by using the scaling renormalization group (RG) approach [12]. Furthermore, we investigate the effect of temperature on the linear conductance and identify ways to pinpoint the regions where Kondo states emerge by analyzing the system's behavior in the two possible magnetic configurations of the leads (parallel or antiparallel). Because an accurate analysis of such effects requires resorting to nonperturbative methods, here we employ the numerical renormalization group (NRG) method [50,51]. We also note that a similar SU(4)-SU(2) crossover caused by an external magnetic field has been recently studied [34]. In our case, however, the crossover takes place due to the proximity effect with ferromagnetic leads in the absence of a magnetic field.

This paper is organized as follows. In Sec. II, we introduce the Hamiltonian of the system under investigation. The renormalization group analysis for the SU(4) \rightarrow SU(2) crossover together with the scaling equations that describe the crossover are presented in Sec. III, while Sec. IV gives details on the NRG procedure and presents how the quantities of interest, such as

*weymann@amu.edu.pl

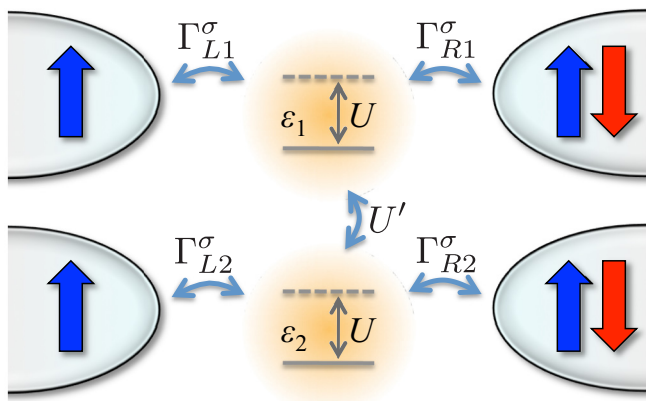


FIG. 1. Schematic of a double quantum dot (DQD) system with ferromagnetic leads. Each dot, with energy level ε_j and Coulomb correlation U , is coupled to a pair of left and right leads with coupling strength Γ_{rj}^σ . The Coulomb correlations between the dots are denoted by U' . The magnetizations of the leads are assumed to form either a parallel (P) or antiparallel (AP) magnetic configuration.

the linear conductance, are computed for different magnetic configurations of the device. Results of the NRG calculations for the $SU(4) \rightarrow SU(2)$ crossover are presented in Sec. V, whereas the general behavior of the linear conductance and the tunnel magnetoresistance is discussed in Sec. VI. The paper is concluded in Sec. VII.

II. MODEL FOR THE DOUBLE DOT SETUP

The setup we consider consists of two capacitively coupled quantum dots, each one coupled to external leads (see the sketch in Fig. 1). Each dot is described by the single-impurity Anderson model (SIAM). We denote by ε_j , with $j = \{1, 2\}$, the energy of an electron residing in dot j . Each dot can accommodate up to two electrons, and they interact with each other through an on-site interaction U and an interdot interaction U' . Their occupation is denoted by $n_{j\sigma} = d_{j\sigma}^\dagger d_{j\sigma}$, with $d_{j\sigma}^\dagger$ creating a spin- σ electron in dot j . The double dot Hamiltonian then reads

$$H_{\text{DQD}} = \sum_{j\sigma} \varepsilon_j n_{j\sigma} + \sum_j U n_{j\uparrow} n_{j\downarrow} + U' (n_{1\uparrow} + n_{1\downarrow})(n_{2\uparrow} + n_{2\downarrow}). \quad (1)$$

In the absence of an external magnetic field, $B = 0$, if the energy levels are degenerate, i.e., $\varepsilon_1 = \varepsilon_2$, and when $U = U'$, the H_{DQD} Hamiltonian is $SU(4)$ invariant¹ [29]. When the orbital degeneracy is lifted, corresponding to a situation when $\varepsilon_1 \neq \varepsilon_2$, H_{DQD} remains $SU(2)$ invariant in the spin sector. For more realistic situations [33], when $U'/U < 1$, the $SU(4)$ symmetry is in general lost. Still, in this case, the system exhibits a special point in the $\{\varepsilon_1, \varepsilon_2\}$ parameter space where an emergent $SU(4)$ symmetry can occur [29], i.e., $\{\varepsilon_1, \varepsilon_2\} \approx$

$\{-U'/2, -U'/2\}$.² This special point will be discussed in more detail in Secs. III and V.

The double dot setup is attached to four external ferromagnetic leads, modeled as reservoirs of noninteracting quasiparticles,

$$H_{\text{Leads}} = \sum_{rj\mathbf{k}\sigma} \varepsilon_{rj\mathbf{k}\sigma} c_{rj\mathbf{k}\sigma}^\dagger c_{rj\mathbf{k}\sigma}. \quad (2)$$

Here, $c_{rj\mathbf{k}\sigma}^\dagger$ is the creation operator for an electron with momentum \mathbf{k} and spin σ in the lead $r = \{L, R\}$ attached to dot j . Consequently, the corresponding local density of states ρ_{rj}^σ becomes spin dependent. Furthermore, this affects the broadening function that describes the coupling between the dots and the leads, i.e., $\Gamma_{rj}^\sigma = \pi \rho_{rj}^\sigma |v_{rj}|^2$, where v_{rj} is the amplitude of the tunneling. The tunneling Hamiltonian is given by

$$H_{\text{Tun}} = \sum_{rj\mathbf{k}\sigma} v_{rj} (c_{rj\mathbf{k}\sigma}^\dagger d_{j\sigma} + d_{j\sigma}^\dagger c_{rj\mathbf{k}\sigma}). \quad (3)$$

It is more convenient to express the couplings in terms of spin polarization of a given lead, p_{rj} , as $\Gamma_{rj}^\sigma = (1 + \sigma p_{rj}) \Gamma_{rj}$, where $\Gamma_{rj} = (\Gamma_{rj}^\uparrow + \Gamma_{rj}^\downarrow)/2$. In the present work, we assume that the magnetizations of the leads are collinear and can take two configurations: (i) parallel (P) and (ii) antiparallel (AP). We also consider that the density of states is flat with the bandwidth given by $2D_0$, and we set $D_0 \equiv 1$ as the energy unit. The total Hamiltonian describing the double dot system coupled to ferromagnetic leads is then given by

$$H = H_{\text{DQD}} + H_{\text{Leads}} + H_{\text{Tun}}. \quad (4)$$

In the following, we will solve it using the Wilson's NRG method [50].

III. THE $SU(4)$ TO $SU(2)$ CROSSOVER IN THE KONDO REGIME

We shall first focus on the special point $\{\varepsilon_1, \varepsilon_2\} = \{-U'/2, -U'/2\}$ that displays the emerging $SU(4)$ Kondo physics (provided $U \gtrsim U'$ [29]) in the limit when the leads are nonmagnetic. For finite spin polarization of the leads, the system's behavior greatly depends on its magnetic configuration. In the case of antiparallel configuration, the effective spin-resolved couplings between given dot and corresponding leads become spin-independent and the ground-state properties of the system are not affected by spin polarization.³ On the other hand, in the parallel configuration, the couplings are spin-dependent, which results in lifting of the spin degeneracy such that only the orbital $SU(2)$ symmetry is preserved. Therefore, in the rest of this section, we shall focus on the case of the parallel magnetic configuration and study the effect of finite p

²For the system to remain $SU(4)$ invariant, it is mandatory for the polarization of the leads to be zero and that there is no hopping between the dots.

³This is the case for left-right symmetric systems. Finite asymmetry can result in spin dependence of the couplings, but then the transport behavior is similar to that in the parallel configuration with some new effective spin polarization [52].

¹The $SU(4)$ symmetry can be constructed as $SU(4) = SU_{\text{spin}}(2) \times SU_{\text{orbital}}(2)$, since H_{DQD} is $SU(2)$ invariant in both the spin and orbital sectors.

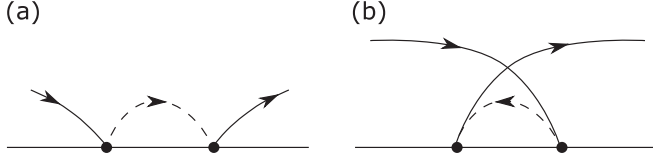


FIG. 2. Second-order diagrams contributing to the renormalization of the coupling matrix displaying processes when a virtual particle is scattered in the upper band edge (a) or a virtual hole in the lower band edge (b) of the lead electrons.

on the system's low-temperature behavior. As already pointed out, by changing the polarization of the external leads from nonmagnetic with $p = 0$ to fully polarized with $p = 1$, it is possible to capture the $SU(4) \rightarrow SU(2)$ Kondo crossover.

To comprehend the essential physics, we map the Hamiltonian (4) to the Kondo model by projecting onto the subspace with single occupancy $\langle n \rangle \simeq 1$ by using the Schrieffer-Wolff transformation [12]. We assume that the dots are symmetrically coupled, $v_{Lj} = v_{Rj} = v_j$ and $p_{Lj} = p_{Rj} = p$. We then make a change of basis by performing a unitary transformation on the leads operators and use an even/odd combination,

$$\begin{pmatrix} c_{ej\mathbf{k}\sigma} \\ c_{oj\mathbf{k}\sigma} \end{pmatrix} = \frac{1}{\sqrt{2}} \begin{pmatrix} 1 & 1 \\ -1 & 1 \end{pmatrix} \begin{pmatrix} c_{Lj\mathbf{k}\sigma} \\ c_{Rj\mathbf{k}\sigma} \end{pmatrix}. \quad (5)$$

In this even-odd basis, the odd channel becomes decoupled and the double dot remains coupled only to the even channel. In what follows, we shall drop the corresponding subscript, i.e., $c_{ej\mathbf{k}\sigma} \rightarrow c_{j\mathbf{k}\sigma}$. We introduce the tensor product notations $(\hat{\sigma}^\mu \otimes \hat{\tau}^\nu)_{j\sigma;j'\sigma'} = \sum_{\mathbf{k}\mathbf{k}'} c_{j\mathbf{k}\sigma}^\dagger \sigma_{\sigma\sigma'}^\mu \tau_{j'j'}^\nu c_{j'\mathbf{k}'\sigma'}$ and $(\hat{S}^\mu \otimes \hat{T}^\nu)_{j\sigma;j'\sigma'} = d_{j\sigma}^\dagger (\frac{1}{2} \sigma_{\sigma\sigma'}^\mu) (\frac{1}{2} \tau_{j'j'}^\nu) d_{j'\sigma'}$, where $\sigma^\mu = \{I_2, \sigma_x, \sigma_y, \sigma_z\}$ are the regular Pauli matrices for $\mu = 1 \rightarrow 3$ and the unit matrix when $\mu = 0$, acting on the spin degrees of freedom, and similar for τ^ν but acting on the orbital part. Then, disregarding the potential scattering, the anisotropic Kondo Hamiltonian can be written as

$$H_K = \sum_{\substack{\sigma\sigma'\alpha\alpha' \\ jj'ii' \\ \mu\nu}} J_{j\sigma;j'\sigma'}^{\mu;\nu} (\hat{\sigma}^\mu \otimes \hat{\tau}^\nu)_{j\sigma;j'\sigma'} (\hat{S}^\mu \otimes \hat{T}^\nu)_{i\alpha;i'\alpha'}. \quad (6)$$

Altogether there are 15 terms in Eq. (6) and the exchange couplings $J_{j\sigma;j'\sigma'}^{\mu;\nu}$ depend on all the parameters of the original Hamiltonian, i.e., ε_j , U , and Γ_{rj}^σ . In the limiting case when $U = U'$ and $p = 0$, it is straightforward to show that all the couplings are equal, $\mathbf{J} \rightarrow J$, and the charge and spin contributions combine in an $SU(4)$ -symmetric way. The $15 = 4^2 - 1$ generators for the $SU(4)$ Lie algebra are $\{I_2, \boldsymbol{\sigma}\} \otimes \{I_2, \boldsymbol{\tau}\} - I_2 \otimes I_2$. On the other hand, when $p = 1$, i.e., the leads are frozen, for example, in the spin- \uparrow state, H_K remains $SU(2)$ invariant in the orbital sector.

To capture the crossover we performed the RG analysis [12] for the exchange couplings \mathbf{J} in between these two fixed points. The second-order processes (particle and holelike) that renormalize the couplings are displayed in Fig. 2. Keeping in mind that the polarization of the leads affects only the spin sector, we can group the couplings into five distinct classes. Furthermore, we define dimensionless couplings by

introducing the local density of states $\rho_0 = 1/2D_0$ as

$$\begin{aligned} j_1 &= \rho_0 J_{j\uparrow;j'\uparrow}^{\mu=\{0,3\};\nu \neq 0}, & j_2 &= \rho_0 J_{j\downarrow;j'\downarrow}^{\mu=\{0,3\};\nu \neq 0}, \\ j_3 &= \rho_0 J_{j\sigma;j'\bar{\sigma}}^{\mu=\{1,2\};\nu}, & j_4 &= \rho_0 J_{j\uparrow;j\uparrow}^{3;0}, \\ j_5 &= \rho_0 J_{j\downarrow;j\downarrow}^{3;0}, \end{aligned} \quad (7)$$

subject to initial conditions $j_1^0 = j_4^0 = \rho_0 J^0(1+p)$, $j_2^0 = j_5^0 = \rho_0 J^0(1-p)$, and $j_3^0 = \rho_0 J^0 \sqrt{1-p^2}$, where $J^0 = v^2(\frac{1}{\varepsilon+U} - \frac{1}{\varepsilon})$ and v is the isotropic coupling.⁴ Here, $2D_0$ is the bandwidth for the conduction electrons. To second order in \mathbf{j} , the scaling equations are easily derived by progressively reducing the bandwidth D [12] as

$$\begin{aligned} \frac{dj_1}{d \ln D} &= -2j_3^2 - 2j_1^2, \\ \frac{dj_2}{d \ln D} &= -2j_3^2 - 2j_2^2, \\ \frac{dj_3}{d \ln D} &= -\frac{3}{2}j_3(j_1 + j_2) - \frac{1}{2}j_3(j_4 + j_5), \\ \frac{dj_4}{d \ln D} &= -4j_3^2, \\ \frac{dj_5}{d \ln D} &= -4j_3^2. \end{aligned} \quad (8)$$

The $SU(4)$ fixed point is captured by setting $p = 0$, implying that all the couplings are the same $j_i = j$, in which case the set (8) of equations collapses to a single one:

$$\frac{dj}{d \ln D} = -4j^2, \quad p \rightarrow 0. \quad (9)$$

In contrast, when the leads are fully spin polarized, $p = 1$, the coupling j_4 remains marginal, the couplings $j_2 = j_3 = j_5 = 0$, while $j = j_1$ rescales accordingly to the regular $SU(2)$ Kondo physics

$$\frac{dj}{d \ln D} = -2j^2, \quad p \rightarrow 1. \quad (10)$$

In a general situation with $0 \leq p \leq 1$, we can solve the RG equations (8) numerically. A typical solution is presented in Fig. 3(a) for $p = 0.8$, and as expected all the couplings diverge at the same characteristic energy scale [12]. In the limit when $p \rightarrow 0$ the curves in Fig. 3(a) collapse to a single one. We define the Kondo temperature T_K as the characteristic energy where the scaling equations (8) diverge. In general, in the $SU(N)$ Kondo model [12], apart from some higher-order corrections [53], the Kondo temperature is given by

$$T_K^{\text{SU}(N)} \simeq D_0 e^{-1/(Nj)}, \quad (11)$$

the expression that can be easily obtained by solving Eqs. (9) and (10) analytically. On the other hand, when the polarization of the leads is changed in between these limits, $0 < p < 1$, T_K changes in a nonmonotonic way. In Fig. 3(b), we represent the evolution of T_K with the spin polarization p of the leads,

⁴In the present calculation, we consider the fully symmetrical situation in which the tunneling amplitudes between each dot and the leads are all identical.

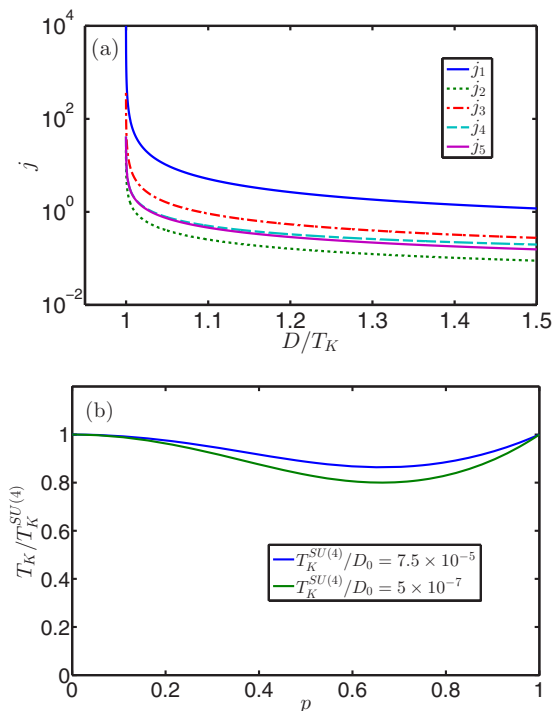


FIG. 3. (a) The renormalization of the coupling constants as the bandwidth is changed. We used $p = 0.8$ and $\rho_0 J^0 = 0.026$. For this choice of parameters, $T_K/D_0 = 6.6 \times 10^{-5}$. (b) The evolution of T_K as a function of spin polarization p . The Kondo temperature is defined here as the energy scale at which the couplings diverge.

which shows that T_K is the same at $p = 0$ and $p = 1$, in agreement with Eq. (11).⁵ When $U \gg U'$, depending on the ratios Γ/U and Γ/U' , the two characteristic energy scales, $T_K^{SU(2)}$ and $T_K^{SU(4)}$, can be well separated, but otherwise the physics remains the same.

To conclude this section, the set (8) of RG equations describes consistently the $SU(4) \rightarrow SU(2)$ crossover and captures the essential Kondo physics in between the two fixed points. In Sec. V, we supplement the RG analysis with more exact numerical renormalization group calculations [50,54] and focus on computing measurable quantities such as the conductance and the tunnel magnetoresistance.

IV. NUMERICAL RENORMALIZATION GROUP AND THE CONDUCTANCE

In this work, we are interested in the linear response transport properties of the system at low enough temperatures such that the electron correlations give rise to the Kondo effect [10,12]. The aim, in particular, is to elucidate the role of spin-dependent tunneling on the transport properties in the full parameter space, with a special focus on the $SU(4)$ Kondo regime [23]. In order to achieve this goal in the most accurate manner, we employ the nonperturbative numerical renormalization group (NRG) method [50,54]. In the NRG approach,

the conduction bands of the noninteracting electrons in the leads are discretized in a logarithmic way with a discretization parameter Λ (here we use $\Lambda = 2$). The discretized Hamiltonian is then transformed to a tight-binding chain Hamiltonian with exponentially decaying hoppings (Wilson chain).

We follow the same strategy as discussed in Sec. III and use the even-odd basis. In this way each dot is coupled to a single channel—the even channel—with a coupling strength, $\Gamma_j^\sigma = \Gamma_{Lj}^\sigma + \Gamma_{Rj}^\sigma$. The NRG Hamiltonian of the system is

$$H_{\text{NRG}} = H_{\text{DQD}} + \sum_{j\sigma} \sqrt{\frac{\Gamma_j^\sigma}{\rho_0 \pi}} (f_{j0\sigma}^\dagger d_{j\sigma} + d_{j\sigma}^\dagger f_{j0\sigma}) + \sum_{jn\sigma} \xi_n (f_{jn\sigma}^\dagger f_{j(n+1)\sigma} + f_{j(n+1)\sigma}^\dagger f_{jn\sigma}). \quad (12)$$

Here, $f_{jn\sigma}^\dagger$ denotes the creation operator of a spin- σ electron at site n ($n = 0, 1, 2, \dots$) of the j^{th} ($j = 1, 2$) Wilson chain and ξ_n are the respective hopping integrals. This Hamiltonian is solved iteratively by retaining an appropriate number N_K of low-energy states at each iteration (here we keep at least $N_K = 10^4$ states). The discarded states, on the other hand, form a complete many-body basis of the whole NRG Hamiltonian [55] and are used to construct the full density matrix of the system [56].

Along the NRG procedure, one needs to deal with a large Hilbert space at each step of iteration, therefore it is crucial to exploit as many symmetries of the NRG Hamiltonian as possible. Here we make use of four Abelian symmetries,⁶ defined by the generators

$$Q_j = \sum_{\sigma} \left(n_{j\sigma} - \frac{1}{2} \right) + \sum_{n\sigma} \left(f_{jn\sigma}^\dagger f_{jn\sigma} - \frac{1}{2} \right), \\ S_z^j = \frac{1}{2} (n_{j\uparrow} - n_{j\downarrow}) + \frac{1}{2} \sum_n (f_{jn\uparrow}^\dagger f_{jn\uparrow} - f_{jn\downarrow}^\dagger f_{jn\downarrow}), \quad (13)$$

for the total charge and z th spin component of dot and chain j , respectively. The quantities we are particularly interested in are (i) the total spectral function

$$A(\omega) = \sum_{j\sigma} A_{j\sigma}(\omega) = -\frac{1}{\pi} \sum_{j\sigma} \text{Im} G_{j\sigma}^R(\omega), \quad (14)$$

with $G_{j\sigma}^R(\omega)$ being the Fourier transform of the retarded Green's function, $G_{j\sigma}^R(t) = -i\Theta(t)\langle\{d_{j\sigma}(t), d_{j\sigma}^\dagger(0)\}\rangle$, and (ii) the linear conductance

$$G = \frac{e^2}{h} \sum_{j\sigma} \frac{4\Gamma_{Lj}^\sigma \Gamma_{Rj}^\sigma}{\Gamma_{Lj}^\sigma + \Gamma_{Rj}^\sigma} \int d\omega \left(-\frac{\partial f(\omega)}{\partial \omega} \right) \pi A_{j\sigma}(\omega), \quad (15)$$

where $f(\omega)$ denotes the Fermi-Dirac distribution function⁷ [59]. To get a clear picture, we assume equal spin polarizations

⁶At some particular points in the stability diagram, the symmetry is higher in the spin and orbital space.

⁷To obtain the relevant spectral functions, we use the usual log-Gaussian broadening kernel [56], however, the conductance is calculated directly from discrete data [57], which makes the results robust against broadening artifacts [58].

⁵Notice that based on Eq. (8) the initial exchange coupling is doubled when $p = 1$ compared to its value for $p = 0$.

of the leads, $p_{rj} \equiv p$, and equal coupling strengths, $\Gamma_{rj} \equiv \Gamma/2$. Then the expression (15) for the linear conductance reduces to

$$G^{\text{AP}} = \frac{2e^2}{h}(1 - p^2)\Gamma \int d\omega \left(-\frac{\partial f(\omega)}{\partial \omega} \right) \pi A^{\text{AP}}(\omega), \quad (16)$$

for the antiparallel (AP) configuration, where $A^{\text{AP}}(\omega)$ denotes the spectral function in the AP configuration, with $A_{j\uparrow}^{\text{AP}}(\omega) = A_{j\downarrow}^{\text{AP}}(\omega)$. As can be seen, G^{AP} is the linear conductance—up to the prefactor $(1 - p^2)$ —of a DQD setup with nonmagnetic leads. Consequently, in the antiparallel configuration, finite spin polarization of the leads results in a reduction of the overall conductance through the system, however, it does not affect its ground-state properties. On the other hand, the conductance in the parallel (P) configuration is given by

$$G^{\text{P}} = \frac{e^2}{h} \sum_{\sigma} (1 + \sigma p) \Gamma \int d\omega \left(-\frac{\partial f(\omega)}{\partial \omega} \right) \pi A_{\sigma}^{\text{P}}(\omega), \quad (17)$$

where $A_{\sigma}^{\text{P}}(\omega) = \sum_j A_{j\sigma}^{\text{P}}(\omega)$ is the spin-dependent spectral function in the parallel configuration. The difference between conductances in the two magnetic alignments can be described by the tunnel magnetoresistance, which is defined as [60,61]

$$\text{TMR} = \frac{G^{\text{P}} - G^{\text{AP}}}{G^{\text{AP}}}. \quad (18)$$

In the present work, we use the NRG to investigate the full phase space of the model. However, to connect to the RG results presented in Sec. III, let us first discuss the $\text{SU}(4) \rightarrow \text{SU}(2)$ crossover and follow the evolution of the spectral functions as well as the conductance—the quantities that were not accessible in the RG approach.

V. THE SU(4) TO SU(2) CROSSOVER: NRG RESULTS

In this section, we focus on the SU(4) Kondo regime and analyze the influence of finite leads' spin polarization on the transport properties. We shall present the results for the spectral functions $A_{\sigma}^{\text{P}}(\omega)$ as well as for the temperature dependence of the conductance.⁸ We will discuss in detail the case of $U = U'$, and later address a more realistic situation when $U > U'$ [33].

An important quantity that captures the crossover is the spectral function, $A_{\sigma}^{\text{P}}(\omega)$, whose spin components are displayed in Figs. 4(a) and 4(b), respectively. The total spectral function itself, $A^{\text{P}}(\omega)$, is presented in the inset of Fig. 4(b). When $p = 0$, it displays the regular SU(4) Kondo resonance formed away from the Fermi level at $\omega \approx T_K^{\text{SU}(4)}$. When increasing the spin polarization, its maximum becomes suppressed and moves toward $\omega = 0$, and when $p = 1$ the orbital-SU(2) Kondo resonance is formed at $\omega = 0$.

We can get more information by inspecting the spin-resolved spectral functions. In the case of spin-up channel, which belongs to the majority-spin subband, increasing the spin polarization results in an enhancement of the spectral

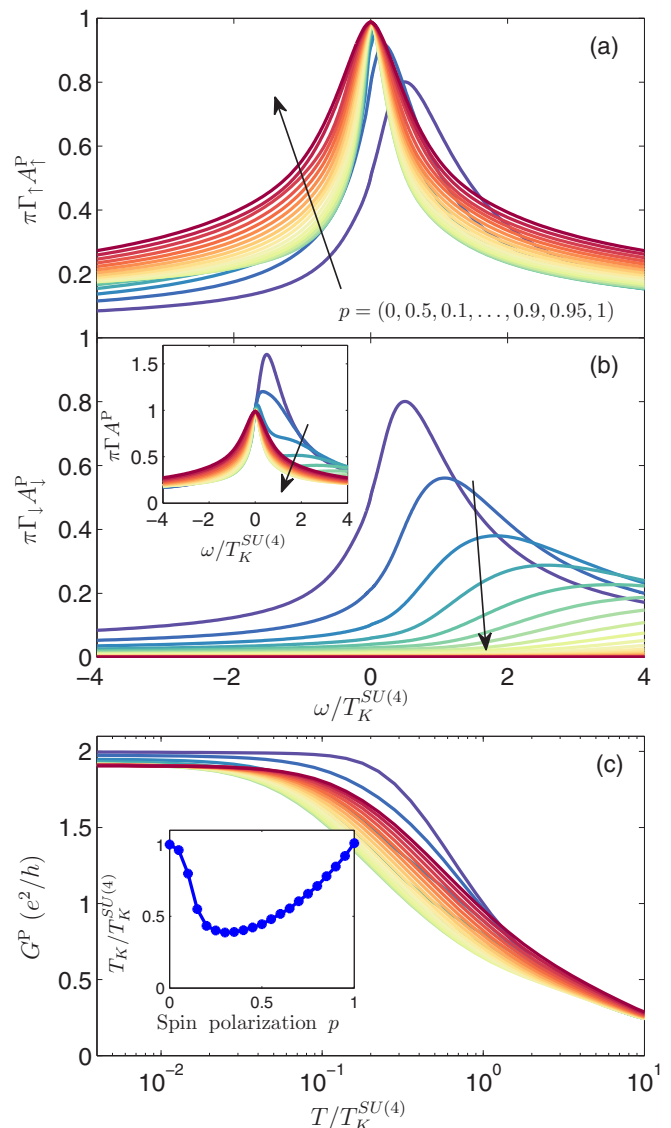


FIG. 4. The energy dependence of (a) the zero-temperature spin-up and (b) spin-down spectral function, together with (c) the linear conductance as a function of temperature calculated for different spin polarizations of the leads, ranging from $p = 0$ to $p = 1$ in steps of 0.05 (the arrow indicates the direction in which p increases), in the SU(4) Kondo regime. The inset in (b) shows the total spectral function, while the inset in (c) presents the Kondo temperature as a function of p . The Kondo temperature is defined by $G(T)/G(T = 0) = 1/2$. $T_K^{\text{SU}(4)} (\approx 2.8 \times 10^{-4}U)$ denotes the SU(4) Kondo temperature (in the case of $p = 0$). The parameters are $U = U' = 0.5$, $\Gamma = 0.015$, in units of band half width, and $\varepsilon_1 = \varepsilon_2 = -U'/2$.

function to $A_{\uparrow}^{\text{P}}(\omega \rightarrow 0) \simeq 1/\pi\Gamma_{\uparrow}$. Moreover, the maximum in $A_{\uparrow}^{\text{P}}(\omega)$ gradually shifts to the Fermi energy, such that for $p = 1$, only the orbital degree of freedom is relevant, and the SU(2) Kondo peak becomes symmetric around $\omega = 0$. On the other hand, $A_{\downarrow}^{\text{P}}(\omega)$ exhibits a completely different behavior. First of all, increasing the spin polarization results in a decrease of $A_{\downarrow}^{\text{P}}(\omega)$. Furthermore, the maximum in the spin-down spectral function moves away from the Fermi energy, due to the development of the exchange field $\Delta\varepsilon_{\text{exch}}$ [36,37] and this

⁸Because the effect of finite p in the antiparallel magnetic configuration is merely limited to a polarization-dependent prefactor, in this section, we focus on the case of the parallel configuration only.

splitting grows with increasing p . Finally, for $p = 1$, $A_{\downarrow}^P(\omega)$ becomes completely quenched at low energies.

This distinct behavior of the spectral function is corroborated with a detailed analysis of the temperature dependence of the linear conductance, which is shown in Fig. 4(c). At the two fixed points (corresponding to $p = 0$ and $p = 1$), the conductance is a universal function of $T/T_K^{\text{SU}(N)}$ [23,33]. Interestingly, despite the fact that the system's ground-state degeneracy becomes reduced from fourfold to twofold, increasing the spin polarization has a rather small effect on the conductance itself. To make the connection to the experiments, from now on we shall use a different definition for the Kondo temperature, $G(T = T_K) = G(T = 0)/2$, i.e., the temperature at which the conductance drops to half of its zero-temperature value.⁹ The evolution of T_K with increasing the spin polarization is presented in the inset of Fig. 4(c). As previously predicted by the RG equations, the polarization of the leads has a relatively small effect on T_K and, consequently, $T_K^{\text{SU}(4)} \approx T_K^{\text{SU}(2)}$. We would, however, like to note that the difference between the two Kondo temperatures can be enlarged by reducing the charge fluctuations, i.e., by decreasing the ratio of Γ/U .

Let us now analyze a more realistic situation when $U > U'$. Now the two Kondo temperatures $T_K^{\text{SU}(N=2,4)}$ are well separated, which allows us to clearly identify the exchange-field-induced splitting in the conductance behavior. This can be obtained by properly tuning the ratio between the couplings and Coulomb correlations. The energy dependence of the spectral function and the temperature dependence of the conductance calculated for $\Gamma/U = 0.015$ are shown in Fig. 5. Since $T_K^{\text{SU}(4)}$ is now much smaller ($T_K^{\text{SU}(4)}/U \approx 7.5 \times 10^{-5}$), a very small spin polarization ($p \gtrsim 0.02$) is sufficient to suppress the SU(4) Kondo effect completely [see Fig. 5(a)]. Quite unexpectedly, the width of the orbital Kondo peak depends in a nonmonotonic fashion on the degree of spin polarization of the leads [see also the inset in Fig. 5(a)], and the minimum width occurs around $p \approx 0.1$.

This behavior is now clearly reflected in the temperature dependence of the conductance shown in Fig. 5(b). The $p = 0$ curve presents a universal SU(4) conductance dependence, which then, with increasing p , smoothly changes to the SU(2) universal curve. Moreover, the extracted Kondo temperature reveals a nonmonotonic dependence on spin polarization. First, the Kondo temperature quickly drops with p and is much lower than $T_K^{\text{SU}(4)}$. Further increase of p , however, results in an enhancement of the SU(2) Kondo temperature. To understand this enhancement, we recall that spin-dependent hybridization (which grows with p), results in DQD level renormalization, such that the position of the spin-up levels becomes effectively lowered. As a consequence, it reduces the excitation energies for the pseudo-spin-flip processes responsible for the Kondo effect, leading to an increase of $T_K^{\text{SU}(2)}$, such that for $p = 1$, one may even achieve $T_K^{\text{SU}(2)} > T_K^{\text{SU}(4)}$, see the inset of Fig. 5(b), which is not in general obvious.

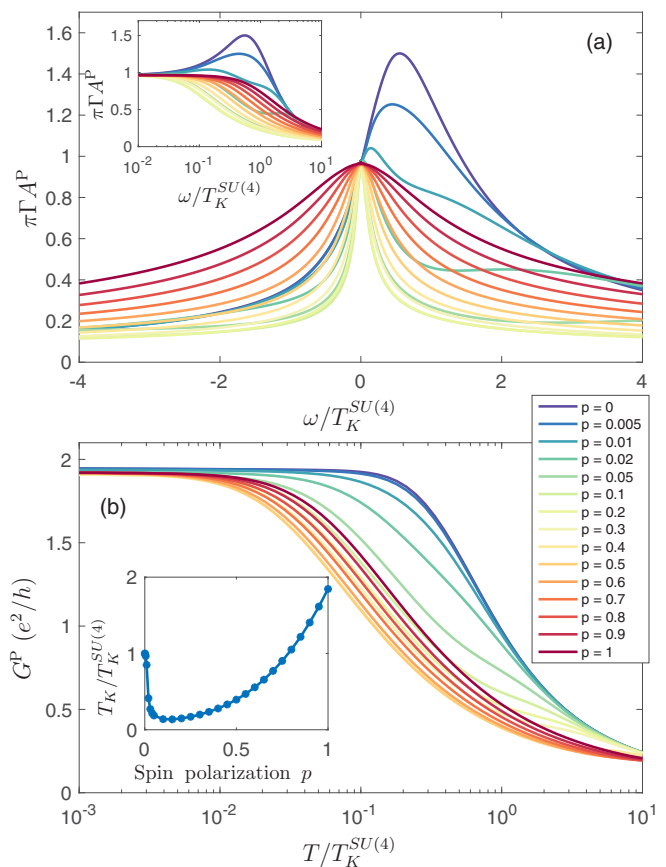


FIG. 5. (a) The energy dependence of the zero-temperature total spectral function and (b) the temperature dependence of the linear conductance calculated for different spin polarizations of the leads, as indicated. The inset in (a) shows the spectral function on the logarithmic scale, while the inset in (b) presents the Kondo temperature as a function of p . The parameters are the same as in Fig. 4 with $U = 1$ and $U' = U/2$. Now $T_K^{\text{SU}(4)}/U \approx 7.5 \times 10^{-5}$.

VI. STABILITY DIAGRAMS AND TUNNEL MAGNETORESISTANCE

In this section, we present results for the low-temperature linear conductance in the parallel and antiparallel configurations, together with the TMR, calculated as a function of the double-dot energy levels ε_1 and ε_2 . In Fig. 6, we present a typical stability diagram that covers the full parameter space, from empty to fully occupied DQD. In this section we address only the regime where $U/U' = 2$.

Let us first discuss the case of the antiparallel magnetic configuration shown in Fig. 6(a). The conductance shows a pattern that closely resembles that of nonmagnetic DQD system [62]. The dashed lines separate the equilibrium charged transport domains. When the number of electrons in each dot is even, the DQD is in a singlet state, no Kondo effect develops and the observed low conductance results only from cotunneling processes. However, when the electron number in either quantum dot is odd, the electronic correlations can give rise to an enhanced conductance due to the Kondo effect, provided the temperature is lower than the Kondo temperature. In our calculations the assumed temperature is very low,

⁹At the $\text{SU}(N = 2, 4)$ fixed points, apart from a numerical prefactor of the order 1, this definition and the one introduced in Eq. (11) give similar values for $T_K^{\text{SU}(N)}$.

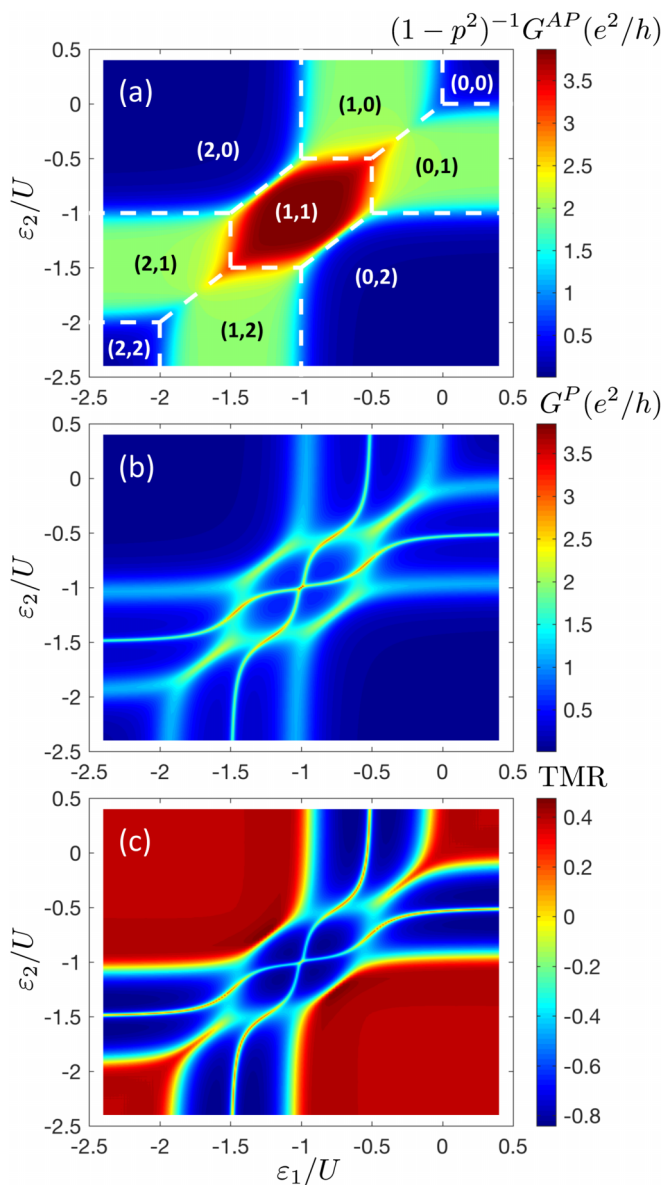


FIG. 6. The linear conductance in (a) the antiparallel and (b) parallel magnetic configuration and (c) the resulting TMR as a function of DQD energy levels ε_1 and ε_2 . The dashed lines in (a) mark the regions where the DQD is in a state (n_1, n_2) with n_1 (n_2) electrons in first (second) dot. The parameters are $U = 1$, $U' = 0.5$, $\Gamma = 0.07$, $p = 0.4$, and $T = 10^{-6}$.

$T \simeq 10^{-6}U$, such that in each Coulomb blockade region the Kondo effect develops.

As the parameter space is relatively large, depending on the nature of the ground state, several types of the Kondo effects develop. When the occupancy of one of the dots is odd, a typical spin-SU(2) Kondo effect develops. This can be observed in transport regime with the electron numbers belonging to the set $\{(1,0), (0,1), (2,1), (1,2)\}$ [see Fig. 6(a)], where $G^{\text{AP}}/(1-p^2)$ reaches the unitary limit $\approx 2e^2/h$. Since there is no direct hopping between the dots, when every dot is singly occupied, $(n_1, n_2) = (1,1)$, one finds that the SU(2) Kondo effect develops independently in each quantum

dot, such that the total conductance reaches $G^{\text{AP}}/(1-p^2) \approx 4e^2/h$.

The stability diagram allows us to get a better understanding of how the emergent SU(4) Kondo effect develops: along the line separating the charge states $(0,1) \leftrightarrow (1,0)$, and $(2,1) \leftrightarrow (1,2)$, besides the spin degeneracy, an additional orbital degeneracy is present and the ground state is fourfold degenerate. Consequently, the system exhibits the SU(4) Kondo effect [33]. As we have seen in Sec. V, the SU(4) Kondo state is better revealed in the parallel configuration, where the spin degeneracy is broken.

The conductance in the parallel configuration is presented in Fig. 6(b) and reveals some huge differences when compared to the AP configuration. This is due to the emergence of the exchange field $\Delta\varepsilon_{\text{exch}}$ that splits the levels of the DQD and lifts the spin degeneracy [63]. As a consequence, since the orbital degeneracy is not affected, one observes the orbital-SU(2) Kondo effect along the lines separating the charge states with occupation $(0,1) \leftrightarrow (1,0)$, and $(1,2) \leftrightarrow (2,1)$ electrons, as well as $(2,0) \leftrightarrow (1,1)$ and $(1,1) \leftrightarrow (0,2)$, see Fig. 6(b). Otherwise, the conductance is generally suppressed except for some special lines where $\Delta\varepsilon_{\text{exch}} \approx 0$.

For example, in the charge sector $(1,0)$, we can understand these particular lines characterized by $\Delta\varepsilon_{\text{exch}} \approx 0$ by computing the effective field $\Delta\varepsilon_{\text{exch}}$ using perturbation theory. Similar to the situation of a single quantum dot [42], we found that the exchange field is linear in spin polarization and is given by

$$\Delta\varepsilon_{\text{exch}}^{(1,0)} \approx \frac{2p\Gamma}{\pi} \ln \frac{|\varepsilon_1|}{|\varepsilon_1 + U|}, \quad (19)$$

independent of ε_2 , and vanishes at the particle-hole symmetry point $\varepsilon_1 = -U/2$. Then, $\Delta\varepsilon_{\text{exch}} \approx 0$, corresponds to the vertical line in the $(1,0)$ sector visible in Fig. 6(c). In the absence of coupling between the two dots, the Kondo effect in the first (second) dot would be thus present for $\varepsilon_1 = -U/2$ ($\varepsilon_2 = -U/2$) for any value of ε_2 (ε_1), resulting in straight vertical and horizontal lines in the $(\varepsilon_1, \varepsilon_2)$ -plane where $\Delta\varepsilon_{\text{exch}} \approx 0$. The expression (19) for $\Delta\varepsilon_{\text{exch}}^{(1,0)}$ is obtained in the simple-minded perturbation theory by building the ground state out of single-particle states. We can do a similar analysis in the $(1,1)$ sector and find that the effective field gets modified into

$$\Delta\varepsilon_{\text{exch}}^{(1,1)} \approx \frac{2p\Gamma}{\pi} \left(\ln \frac{|\varepsilon_1 + U'|}{|\varepsilon_1 + U' + U|} + \ln \frac{|\varepsilon_2 + U'|}{|\varepsilon_2 + U' + U|} \right), \quad (20)$$

which vanishes in the middle of the $(1,1)$ region, in agreement with the results presented in Fig. 6(c). In the crossover region, the ground state becomes a many-body singlet built out of the dot and lead states. Here, higher-order processes are relevant and the simple perturbative estimate for $\Delta\varepsilon_{\text{exch}}$ fails. Still, numerically, we can find the lines where the exchange field vanishes. In the presence of capacitive coupling between the dots, the exact $\Delta\varepsilon_{\text{exch}} \approx 0$ lines become distorted by the interdot Coulomb correlations U' across the separation line between different charge regions, and interpolate between Eqs. (20) and (19), for example, when we cross the $(1,1)$ – $(1,0)$ border.

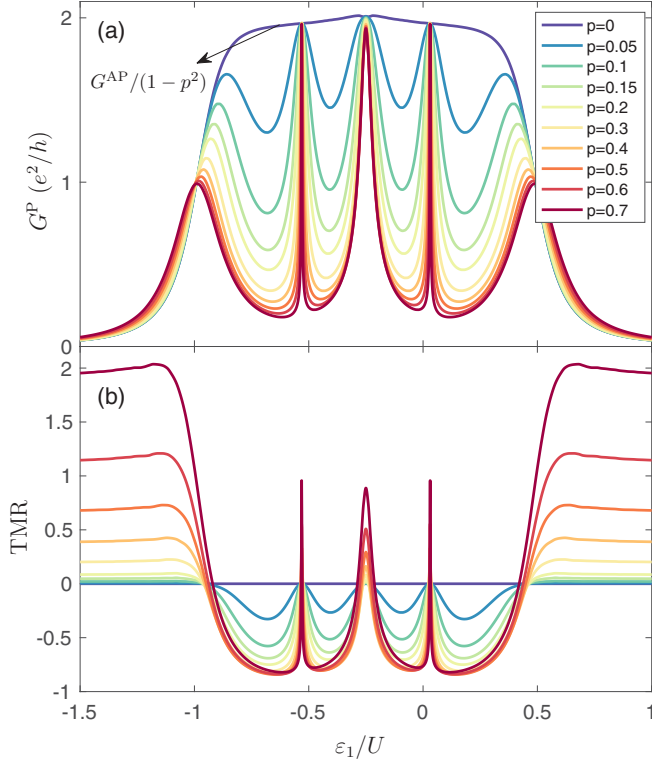


FIG. 7. (a) The linear conductance in both magnetic configurations and (b) the resulting TMR as a function of ϵ_1 with $\epsilon_2 = -\epsilon_1 - U'$ calculated for different values of leads' spin polarization p , as indicated. The conductance in the antiparallel configuration is given by the curve for $p = 0$ multiplied with a factor of $(1 - p^2)$, cf. Eq. (16). The parameters are the same as in Fig. 6.

The difference in conductance in the two magnetic configurations is reflected in the TMR, which is shown in Fig. 6(c). For transport regimes with even occupancy of each dot, elastic cotunneling processes dominate the current and the TMR is given by [64] $\text{TMR} \approx 2p^2/(1 - p^2)$. For odd occupancy, the Kondo effect is present in the case of antiparallel configuration, while in the parallel configuration it is suppressed by the exchange field, such that $G^P \ll G^{AP}$ and $\text{TMR} \rightarrow -1$ [43]. On the other hand, for such values of ϵ_1 and ϵ_2 that the exchange field vanishes, one has $G^{AP}/G^P = 1 - p^2$, which yields $\text{TMR} = p^2/(1 - p^2)$, a ratio which is valid irrespective of the SU(2) or SU(4) Kondo regimes.

To understand the influence of ferromagnetic leads on transport, in the following, we will analyze the behavior of the conductance and the TMR as a function of spin polarization of the leads, as well as temperature along different cuts in the stability diagram. We shall consider two such cross-sections defined as (i) $\epsilon_2 + \epsilon_1 = -U'$ and (ii) $\epsilon_1 = \epsilon_2$, in the stability diagram. In what follows we shall label them cut (line) 1 and 2.

A. Conductance and TMR along cross-sections

The linear conductance in both magnetic configurations and the TMR calculated as a function of ϵ_1 with $\epsilon_2 + \epsilon_1 = -U'$ for different values of spin polarization p are shown in Fig. 7. By changing the level position, the occupation of the DQD changes from (2,0) for $\epsilon_1 \lesssim -U$, to (1,0) for $-U \lesssim$

$\epsilon_1 \lesssim -U'/2$, (0,1) for $-U'/2 \lesssim \epsilon_1 \lesssim U/2$, and to (0,2) for $\epsilon_1 \gtrsim U/2$. In the nonmagnetic lead case, in the odd occupancy regime, the regular spin-SU(2) Kondo effect develops with conductance reaching $\approx 2e^2/h$, see Fig. 7(a). Moreover, for $\epsilon_1 = -U'/2$, an additional orbital degeneracy occurs and the system exhibits the SU(4) Kondo effect, but the conductance remains $G \approx 2e^2/h$. These different types of the Kondo effects are hardly distinguishable by the conductance itself when $T \ll \{T_K^{\text{SU}(2)}, T_K^{\text{SU}(4)}\}$, as it remains close to the unitary value, $G \approx 2e^2/h$ in the whole singly occupied DQD regime, see Fig. 7(a). However, they can be revealed at larger temperatures, i.e., $T \gtrsim \{T_K^{\text{SU}(2)}, T_K^{\text{SU}(4)}\}$ or in the case of ferromagnetic leads.

When $p > 0$, the conductance gets modified. The behavior in the AP configuration is still featureless, similar to the case of normal leads as $G^{AP}(p) = G^{AP}(p=0)(1 - p^2)$. However, the conductance in the P configuration reveals a nontrivial interplay between the spin-resolved DQD level renormalization and the correlations bringing about the Kondo effect. With increasing the spin polarization, the strength of the exchange field increases and once $|\Delta\epsilon_{\text{exch}}|$ becomes larger than the corresponding Kondo scale, the conductance drops. This can be observed in the whole odd occupation regime shown in Fig. 7, i.e., for $-U \lesssim \epsilon_1 \lesssim U/2$, except for some special values of the level position where, again, $\Delta\epsilon_{\text{exch}} \approx 0$. For $\epsilon_1 \approx -U/2$, the exchange field in the first dot vanishes, while for $\epsilon_1 = 0$ (corresponding to $\epsilon_2 \approx -U/2$) the exchange field in the second dot vanishes. As a result, the total conductance reveals two peaks for $\epsilon_1 \approx \{-U/2, 0\}$ with an almost unitary conductance $G^P \approx 2e^2/h$. The height of these peaks remains almost constant, but their width depends on p , as the exchange field increases with p , and a smaller detuning is needed for the condition $|\Delta\epsilon_{\text{exch}}| \gtrsim T_K^{\text{SU}(2)}$ to be fulfilled. In addition, a spin-polarization independent resonance is also present for $\epsilon_1 = -U'/2$ (note that then $\epsilon_2 = \epsilon_1$). This is exactly the special point we have analyzed in Sec. III that shows the SU(4) to SU(2) crossover. Although the maximum value of conductance does not depend at this point on the polarization p , the system's ground state does change. For $p = 0$, it exhibits fourfold degeneracy, which becomes reduced to twofold degeneracy when increasing spin polarization. Consequently, the SU(4) Kondo effect becomes reduced to the orbital SU(2) Kondo effect once $|\Delta\epsilon_{\text{exch}}| \gtrsim T_K^{\text{SU}(4)}$. The width of the resonance for $\epsilon_1 \approx -U'/2$ is determined by the condition $|\Delta\epsilon| \approx T_K^{\text{SU}(2)}$, where $\Delta\epsilon = \epsilon_2 - \epsilon_1$ corresponds to the pseudo-Zeeman splitting.¹⁰

The ϵ_1 dependence of the TMR for different spin polarizations along the first cut we consider is shown in Fig. 7(b). The transport regimes discussed above are clearly visible. In the even occupation regime, the TMR is given by $\text{TMR} = 2p^2/(1 - p^2)$, while in the case of odd DQD occupation, the TMR drops to $\text{TMR} = -1$ with increasing p , except for $\epsilon_1 = -U/2$, $\epsilon_1 = -U'/2$, and $\epsilon_1 = 0$, where $\text{TMR} = p^2/(1 - p^2)$.

Let us now analyze the transport behavior along the second cut, where $\epsilon_1 = \epsilon_2 \equiv \epsilon$. Along this line, when $\epsilon \gtrsim 0$, the DQD is empty, for $-U' \lesssim \epsilon \lesssim 0$, it is singly occupied, for

¹⁰Here, $T_K^{\text{SU}(2)}$ denotes the Kondo temperature of the orbital Kondo effect.

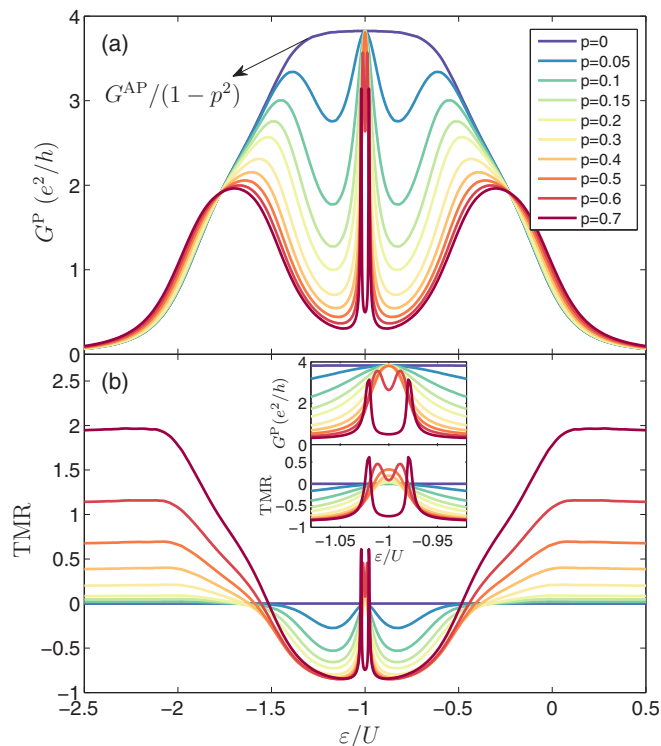


FIG. 8. (a) The linear conductance in both magnetic configurations and (b) the resulting TMR as a function of $\varepsilon_1 = \varepsilon_2 \equiv \varepsilon$ calculated for different values of leads' spin polarization p , as indicated. The inset shows the zoom into the transport regime around $\varepsilon = -U/2 - U'$. The conductance in the antiparallel configuration is given by the curve for $p = 0$ multiplied with a factor of $(1 - p^2)$, cf. Eq. (16). The parameters are the same as in Fig. 6.

$-U - U' \lesssim \varepsilon \lesssim -U'$, two electrons occupy the DQD, when $-2U \lesssim \varepsilon \lesssim -U - U'$, there are three electrons in the DQD, while for $\varepsilon \lesssim -2U$ the DQD is fully occupied with four electrons. In the odd occupation regime, the ground state has fourfold degeneracy and the system exhibits the SU(4) Kondo effect in the case of nonmagnetic leads. A plateau of $G \approx 2e^2/h$ associated with the SU(4) Kondo effect is hardly visible as a function of ε , see the curve for $p = 0$ in Fig. 8(a). This is because of a relatively large Γ/U ratio considered in calculations and the usual spin SU(2) Kondo effect, which develops in both quantum dots yielding $G = 4e^2/h$ in the two-electron regime in the case of $p = 0$. For finite p , in the parallel configuration, the conductance becomes, however, suppressed, except for $\varepsilon \approx -U/2 - U'$, cf. Fig. 6(b), where the exchange field cancels and the Kondo phenomenon can develop. Moreover, the two plateaus in the odd-electron regime, associated with the orbital SU(2) Kondo effect, are clearly visible, see, e.g., the case of $p = 0.7$ in Fig. 8(a). This confirms that for $p = 0$, i.e., in the absence of level spin splitting, the ground state of the system was indeed fourfold degenerate.

Another feature in the ε dependence of the conductance can be seen around $\varepsilon = -U/2 - U'$ for finite p , see Fig. 8(a). As already mentioned, when $\varepsilon \approx -U/2 - U'$, the exchange field vanishes and one should observe the Kondo effect. However, instead of a peak at $\varepsilon \approx -U/2 - U'$, with increasing p , a dip

develops with two small satellite peaks. This effect is associated with an interplay between finite temperature, exchange field, and the Kondo temperature. First of all, one should note that exchange field can be tuned not only by changing the DQD levels (by inducing detuning from $\varepsilon = -U/2 - U'$), but it also grows with spin polarization [42]. Thus, for larger p , a smaller detuning from the point $\varepsilon = -U/2 - U'$ is needed to suppress the Kondo-enhanced conductance, see the width of G^P in the inset in Fig. 8. On the other hand, increasing the spin polarization results in lowering of the corresponding Kondo temperature [36] and, once $T_K \lesssim T$, the conductance becomes suppressed at $\varepsilon = -U/2 - U'$. The crucial observation is that T_K also depends on detuning from the particle-hole symmetry point $\varepsilon = -U/2 - U'$ and grows with increasing this detuning. As a consequence, small side peaks, on either side of $\varepsilon = -U/2 - U'$, develop in G^P for such values of ε that $T_K \approx T$. Note that these peaks are visible as long as $T_K \gtrsim |\Delta\varepsilon_{\text{exch}}|$, and once this condition is not met any more, which happens for even larger p , G^P becomes suppressed.

The corresponding dependence of the TMR is shown in Fig. 8(b). In this figure one can clearly identify all the TMR values discussed earlier. In the empty and fully occupied DQD regime, the elastic cotunneling gives rise to $\text{TMR} = 2p^2/(1 - p^2)$. In the odd occupation regime, the TMR value drops by a factor of 2, while in the case of $-U - U' < \varepsilon < -U'$ the TMR is generally suppressed by the exchange field, $\text{TMR} \rightarrow -1$, except for the middle of the Coulomb diamond, i.e., around $\varepsilon = -U/2 - U'$. There, for large spin polarization, the TMR displays two peaks on either side of $\varepsilon = -U/2 - U'$, see the inset in Fig. 8(b), resulting from the corresponding peaks in G^P . The finite temperature effects visible in Fig. 8 lead our discussion to the analysis of transport properties at different temperatures. This is presented in the next section.

B. Finite temperature effects

In this section, we discuss the effect of the temperature on the linear conductance and TMR. For that we evaluated the conductance in both AP and P magnetic configurations at various temperatures along the two cuts discussed in Sec. VIA. In Fig. 9, we display the evolution of the conductance along the first cross-section, ε_1 with $\varepsilon_2 + \varepsilon_1 = -U'$.

At low temperatures, i.e., $T \lesssim \{T_K^{\text{SU}(4)}, T_K^{\text{SU}(2)}\}$, the conductance in the antiparallel configuration exhibits a plateau in the singly occupied DQD transport regime.¹¹ This plateau changes when the temperature is increased. First, the conductance becomes suppressed in the SU(2) Kondo regime, and at some intermediate temperature, $T_K^{\text{SU}(4)} \gtrsim T \gtrsim T_K^{\text{SU}(2)}$, the resonances at $\varepsilon_1 \approx -U$ and $\varepsilon_1 \approx U/2$ survive, together with the SU(4) Kondo peak at $\varepsilon_1 \approx -U'/2$. From their temperature dependence one can also estimate the Kondo temperatures: in the middle of the spin SU(2) Kondo valley and for parameters assumed in Fig. 9(a), one finds $T_K^{\text{SU}(2)}/U \approx 8.96 \times 10^{-4}$, while the SU(4) Kondo temperature for $\varepsilon_1 \approx -U'/2$, $T_K^{\text{SU}(4)}/U \approx 0.044$.

On the other hand, the evolution of $G^P(T)$ along the first cut is completely different: the Kondo plateau is not present at

¹¹For the parameters that we used, $T_K^{\text{SU}(4)} < T_K^{\text{SU}(2)}$.

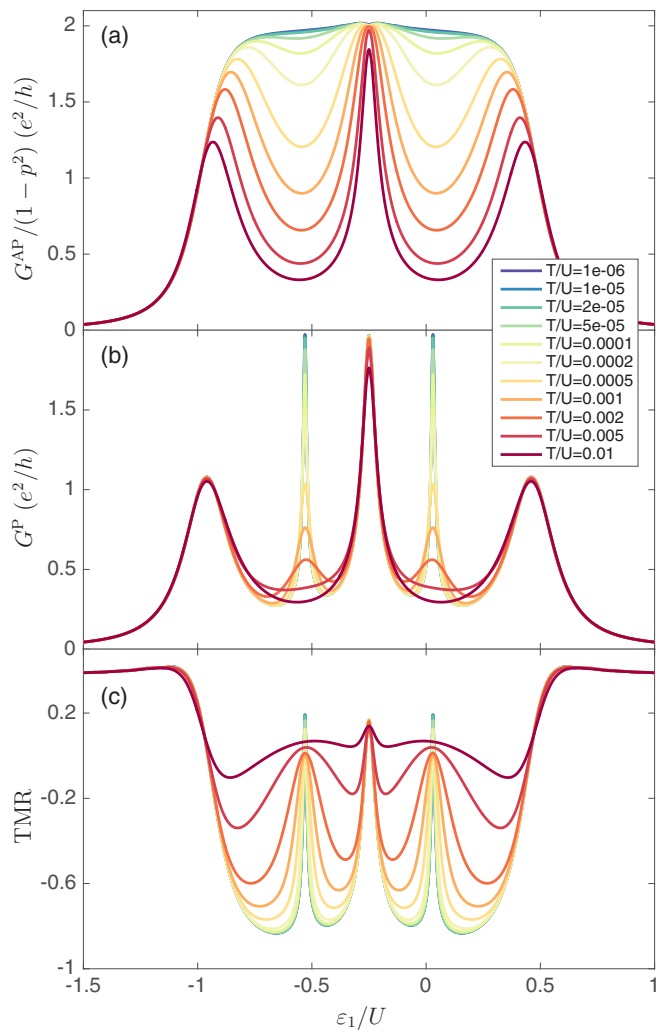


FIG. 9. The linear conductance in (a) the antiparallel and (b) parallel magnetic configurations, as well as (c) the resulting TMR as a function of ε_1 with $\varepsilon_2 = -\varepsilon_1 - U'$ calculated for different temperatures, as indicated. The other parameters are the same as in Fig. 6.

low temperatures, but only some narrow peaks occur at some specific values of ε_1 . It is obvious that the ones occurring at $\varepsilon_1 \approx -U/2$ and $\varepsilon_1 \approx 0$ are associated with the spin-SU(2) Kondo effect.¹² Note that in the case of finite p , the Kondo temperature decreases with increasing spin polarization [36]. Although, based on the previous analysis, we can safely attribute the feature at $\varepsilon_1 \approx -U'/2$ to the SU(4) Kondo effect, from the evolution of G^{P} itself it is not that straightforward to decide what type of correlations causes the conductance enhancement: if $|\Delta\varepsilon_{\text{exch}}| \lesssim T_K^{\text{SU}(4)}$, then the SU(4) nature of the ground state is relevant, whereas for $|\Delta\varepsilon_{\text{exch}}| \gtrsim T_K^{\text{SU}(4)}$, the spin degeneracy is lifted and only the orbital degrees of freedom are degenerate, resulting in orbital Kondo effect. In fact, for parameters assumed in Fig. 9(b), the strength of the exchange field is comparable to $T_K^{\text{SU}(4)}$.

¹²We can also use $G^{\text{P}}(T)$ to estimate the Kondo scale. Here we estimate the Kondo temperature to be $T_K^{\text{SU}(2)}/U \approx 5.89 \times 10^{-4}$.

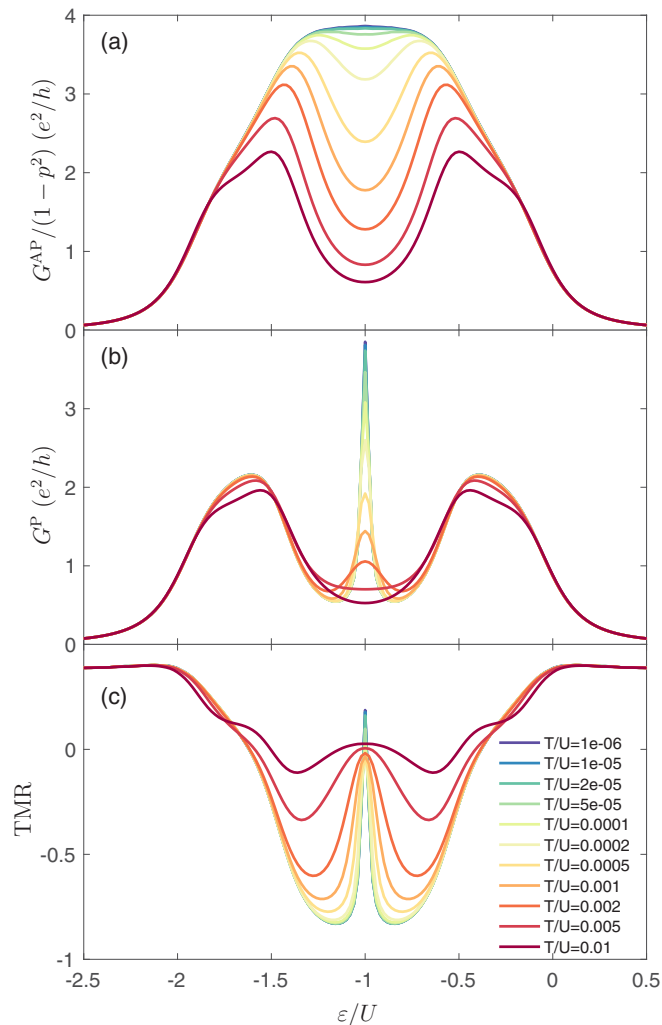


FIG. 10. The linear conductance in (a) the antiparallel and (b) parallel magnetic configurations, as well as (c) the resulting TMR as a function of $\varepsilon_1 = \varepsilon_2 \equiv \varepsilon$ calculated for different temperatures, as indicated. The other parameters are the same as in Fig. 6.

The effects of finite temperature on transport behavior along the second cut we considered ($\varepsilon_1 = \varepsilon_2 \equiv \varepsilon$) are presented in Fig. 10. In the case of antiparallel configuration, the conductance in the middle Coulomb blockade regime becomes quickly suppressed with increasing temperature. However, in the SU(4) Kondo regime, the dependence of G on T is weak in the considered temperature range, since even for the highest temperature considered $T \lesssim T_K^{\text{SU}(4)}$. A similar tendency can be observed in the case of parallel alignment. A strong temperature dependence is only revealed for the Kondo peak at $\varepsilon_1 = -U/2 - U'$, while in the other transport regimes the linear conductance only weakly depends on T .

Finally, the TMR evaluated at various temperatures along the two cross-sections is shown in Figs. 9(c) and 10(c). In these figures one can clearly identify all the TMR values discussed earlier. The general conclusion is that with increasing the temperature, TMR extrema become suppressed, such that in the very high temperature limit ($T \gtrsim U$, not shown), the TMR would be independent of ε_1 and ε_2 , i.e., $\text{TMR} \approx p^2/(1-p^2)$ [43].

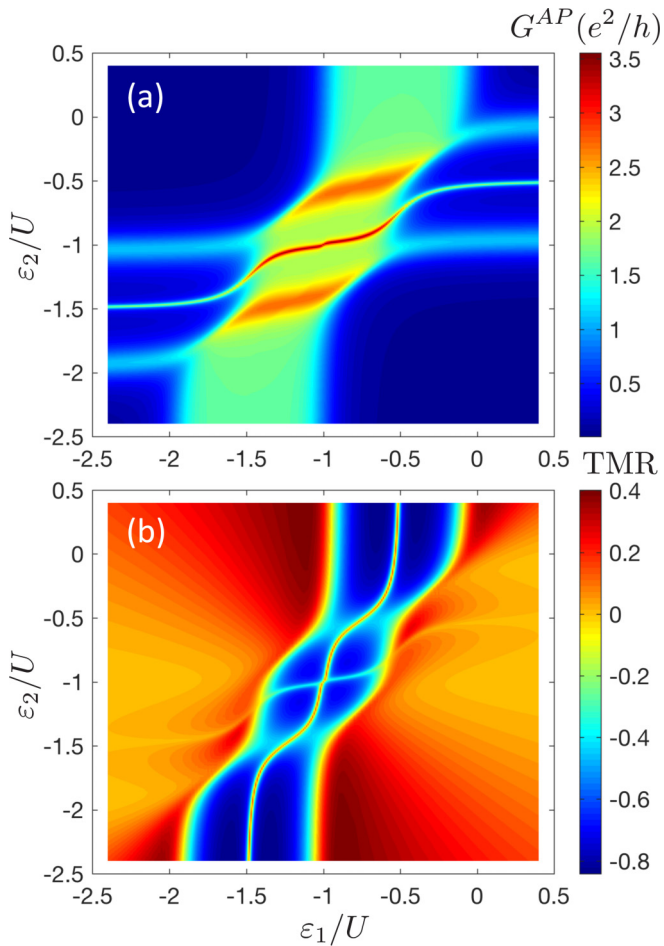


FIG. 11. (a) The linear conductance in the *mixed* antiparallel configuration and (b) the TMR as a function of DQD energy levels. The parameters are same as in Fig. 6. In the *mixed* antiparallel configuration, the magnetization of one of the leads attached to the first dot is opposite to the other leads' magnetizations.

C. Ferromagnets with different coercive fields

In this section, we discuss the magnetoresistive properties of the device assuming an experimentally relevant situation, when the coercive fields of the ferromagnetic electrodes are different. For sufficiently strong magnetic field (but still much smaller than the field necessary to induce a considerable Zeeman splitting), the magnetizations of all electrodes are aligned (parallel configuration). So far, in our analysis, we have assumed that there is a difference between coercive fields of the left and right electrodes, such that at a certain field the leads on one side of the junction flip their magnetizations and the antiparallel configuration occurs, see Fig. 1. However, it may happen that only one of the electrodes flips its magnetic moment, resulting in a *mixed* antiparallel configuration: for example, the leads coupled to the first dot are in the antiparallel, while the leads attached to the second one are in the parallel magnetic configuration. The transport characteristics for such a situation are shown in Fig. 11. One can still identify charged stability regions separated by lines with large conductance: When changing ε_1 , the system exhibits a Kondo plateau (visible in the transport regions for $\varepsilon_2 \lesssim -U - U'$ and $\varepsilon_2 \gtrsim -U'$),

while the characteristic suppression of the Kondo resonance by the exchange field occurs as a function of ε_2 , see Fig. 11(a). The total conductance shows then an enhancement to $G^{AP} = 4e^2(1 - p^2/2)/h$ for such position of the DQD levels that the exchange field on the second dot vanishes. The whole DQD level dependence of conductance in the *mixed* configuration can be understood based on the analysis presented in Sec. VIA, and it results in the associated behavior of the TMR, which is shown in Fig. 11(b).

VII. CONCLUSIONS

In this paper, we studied the linear-response transport properties of a double quantum dot system coupled to ferromagnetic leads in the Kondo regime. The emphasis was put on the transport regime where the system exhibits the SU(4) Kondo effect, which was thoroughly studied against different material parameters of ferromagnetic contacts and magnetic configurations of the device. The calculations were performed with the nonperturbative numerical renormalization group method and supplemented by an RG analysis to describe the SU(4) to SU(2) crossover. We demonstrated that the transport behavior becomes greatly modified when the magnetic configuration of the device changes from the antiparallel to the parallel one, which is a direct consequence of the exchange field induced DQD level splitting. This splitting generally breaks the spin-SU(2) invariance, such that the system exhibits the orbital-SU(2) Kondo effect in corresponding transport regimes.

We systematically investigated the evolution of the spectral functions from the SU(4) to the orbital-SU(2) Kondo regime upon increasing the leads' spin polarization p . Interestingly, the corresponding Kondo temperature reveals then a nonmonotonic dependence on p . First, with increasing spin polarization, the Kondo temperature drops, which is related to the reduction of the fourfold degeneracy to the twofold one. However, further increase of p results in an enhancement of the orbital Kondo temperature, such that for large spin polarization it may even exceed the SU(4) Kondo temperature. This behavior is completely different compared to the single quantum dot case when a monotonic dependence of the spin-SU(2) Kondo temperature on the spin polarization was predicted at the particle-hole symmetry point [36].

Finally, we also analyzed the magnetoresistive properties of the device in the case when the ferromagnets have different coercive fields, such that *mixed* antiparallel configuration is formed. In such a case, the transport behavior is a result of contributions from the parallel and antiparallel configurations of both quantum dots.

ACKNOWLEDGMENTS

This work was supported by the National Science Centre in Poland through the Project No. DEC-2013/10/E/ST3/00213 and by the Romanian National Authority for Scientific Research and Innovation, UEFISCDI, Projects No. PN-II-RU-TE-2014-4-0432 and No. PN-III-P4-ID-PCE-2016-0032. Computing time at the Poznań Supercomputing and Networking Center is acknowledged.

- [1] R. H. Blick, R. J. Haug, J. Weis, D. Pfannkuche, K. V. Klitzing, and K. Eberl, Single-electron tunneling through a double quantum dot: The artificial molecule, *Phys. Rev. B* **53**, 7899 (1996).
- [2] F. R. Waugh, M. J. Berry, D. J. Mar, R. M. Westervelt, K. L. Campman, and A. C. Gossard, Single-Electron Charging in Double and Triple Quantum Dots with Tunable Coupling, *Phys. Rev. Lett.* **75**, 705 (1995).
- [3] J. J. Palacios and P. Hawrylak, Correlated few-electron states in vertical double-quantum-dot systems, *Phys. Rev. B* **51**, 1769 (1995).
- [4] R. Ziegler, C. Bruder, and H. Schoeller, Transport through double quantum dots, *Phys. Rev. B* **62**, 1961 (2000).
- [5] W. G. van der Wiel, S. De Franceschi, J. M. Elzerman, T. Fujisawa, S. Tarucha, and L. P. Kouwenhoven, Electron transport through double quantum dots, *Rev. Mod. Phys.* **75**, 1 (2002).
- [6] D. T. McClure, L. DiCarlo, Y. Zhang, H.-A. Engel, C. M. Marcus, M. P. Hanson, and A. C. Gossard, Tunable Noise Cross Correlations in a Double Quantum Dot, *Phys. Rev. Lett.* **98**, 056801 (2007).
- [7] K. Ono, D. G. Austing, Y. Tokura, and S. Tarucha, Current rectification by pauli exclusion in a weakly coupled double quantum dot system, *Science* **297**, 1313 (2002).
- [8] J. Fransson and M. Rasander, Pauli spin blockade in weakly coupled double quantum dots, *Phys. Rev. B* **73**, 205333 (2006).
- [9] I. Weymann, Effects of different geometries on the conductance, shot noise, and tunnel magnetoresistance of double quantum dots, *Phys. Rev. B* **78**, 045310 (2008).
- [10] J. Kondo, Resistance minimum in dilute magnetic alloys, *Prog. Theor. Phys.* **32**, 37 (1964).
- [11] P. Nozieres and A. Blandin, Kondo effect in real metals, *J. Phys. France* **41**, 193 (1980).
- [12] A. C. Hewson, *The Kondo Problem to Heavy Fermions* (Cambridge University Press, Cambridge, 1993).
- [13] D. L. Cox and A. Zawadowski, Exotic kondo effects in metals: Magnetic ions in a crystalline electric field and tunneling centres, *Adv. Phys.* **47**, 599 (1998).
- [14] M. Pustilnik and L. I. Glazman, Kondo Effect in Real Quantum Dots, *Phys. Rev. Lett.* **87**, 216601 (2001).
- [15] M. Vojta, R. Bulla, and W. Hofstetter, Quantum phase transitions in models of coupled magnetic impurities, *Phys. Rev. B* **65**, 140405 (2002).
- [16] W. G. van der Wiel, S. De Franceschi, J. M. Elzerman, S. Tarucha, L. P. Kouwenhoven, J. Motohisa, F. Nakajima, and T. Fukui, Two-Stage Kondo Effect in a Quantum Dot at a High Magnetic Field, *Phys. Rev. Lett.* **88**, 126803 (2002).
- [17] N. J. Craig, J. M. Taylor, E. A. Lester, C. M. Marcus, M. P. Hanson, and A. C. Gossard, Tunable nonlocal spin control in a coupled-quantum dot system, *Science* **304**, 565 (2004).
- [18] P. S. Cornaglia and D. R. Grempel, Strongly correlated regimes in a double quantum dot device, *Phys. Rev. B* **71**, 075305 (2005).
- [19] S. Sasaki, H. Tamura, T. Akazaki, and T. Fujisawa, Fano-Kondo Interplay in a Side-Coupled Double Quantum Dot, *Phys. Rev. Lett.* **103**, 266806 (2009).
- [20] R. Žitko, Fano-kondo effect in side-coupled double quantum dots at finite temperatures and the importance of two-stage kondo screening, *Phys. Rev. B* **81**, 115316 (2010).
- [21] Y. Tanaka, N. Kawakami, and A. Oguri, Crossover between two different kondo couplings in side-coupled double quantum dots, *Phys. Rev. B* **85**, 155314 (2012).
- [22] P. Petit, C. Feuillet-Palma, M. L. D. Rocca, and P. Lafarge, Universality of the two-stage kondo effect in carbon nanotube quantum dots, *Phys. Rev. B* **89**, 115432 (2014).
- [23] L. Borda, G. Zarand, W. Hofstetter, B. I. Halperin, and J. von Delft, $Su(4)$ Fermi Liquid State and Spin Filtering in a Double Quantum Dot System, *Phys. Rev. Lett.* **90**, 026602 (2003).
- [24] T. Sato and M. Eto, Numerical renormalization group studies of $su(4)$ kondo effect in quantum dots, *Physica E* **29**, 652 (2005).
- [25] M. R. Galpin, D. E. Logan, and H. R. Krishnamurthy, Quantum Phase Transition in Capacitively Coupled Double Quantum Dots, *Phys. Rev. Lett.* **94**, 186406 (2005).
- [26] R. López, D. Sánchez, M. Lee, M.-S. Choi, P. Simon, and K. Le Hur, Probing spin and orbital Kondo effects with a mesoscopic interferometer, *Phys. Rev. B* **71**, 115312 (2005).
- [27] M. R. Galpin, D. E. Logan, and H. R. Krishnamurthy, Renormalization group study of capacitively coupled double quantum dots, *J. Phys.: Condens. Matter* **18**, 6545 (2006).
- [28] S. Amasha, A. J. Keller, I. G. Rau, A. Carmi, J. A. Katine, H. Shtrikman, Y. Oreg, and D. Goldhaber-Gordon, Pseudospin-Resolved Transport Spectroscopy of the Kondo Effect in a Double Quantum Dot, *Phys. Rev. Lett.* **110**, 046604 (2013).
- [29] Y. Nishikawa, A. C. Hewson, D. J. G. Crow, and J. Bauer, Analysis of low-energy response and possible emergent $su(4)$ kondo state in a double quantum dot, *Phys. Rev. B* **88**, 245130 (2013).
- [30] D. A. Ruiz-Tijerina, E. Vernek, and S. E. Ulloa, Capacitive interactions and kondo effect tuning in double quantum impurity systems, *Phys. Rev. B* **90**, 035119 (2014).
- [31] E. Vernek, C. A. Busser, E. V. Anda, A. E. Feiguin, and G. B. Martins, Spin filtering in a double quantum dot device: Numerical renormalization group study of the internal structure of the kondo state, *Appl. Phys. Lett.* **104**, 132401 (2014).
- [32] Y. Nishikawa, O. J. Curtin, A. C. Hewson, D. J. G. Crow, and J. Bauer, Conditions for observing emergent $su(4)$ symmetry in a double quantum dot, *Phys. Rev. B* **93**, 235115 (2016).
- [33] A. J. Keller, S. Amasha, I. Weymann, C. P. Moca, I. G. Rau, J. A. Katine, H. Shtrikman, G. Zarand, and D. Goldhaber-Gordon, Emergent $su(4)$ kondo physics in a spin-charge-entangled double quantum dot, *Nat. Phys.* **10**, 145 (2014).
- [34] V. Lopes, R. A. Padilla, G. B. Martins, and E. V. Anda, $SU(4)$ - $SU(2)$ crossover and spin-filter properties of a double quantum dot nanosystem, *Phys. Rev. B* **95**, 245133 (2017).
- [35] K. Wrześniewski and I. Weymann, Kondo physics in double quantum dot based Cooper pair splitters, *Phys. Rev. B* **96**, 195409 (2017).
- [36] J. Martinek, Y. Utsumi, H. Imamura, J. Barnaś, S. Maekawa, J. König, and G. Schön, Kondo Effect in Quantum Dots Coupled to Ferromagnetic Leads, *Phys. Rev. Lett.* **91**, 127203 (2003).
- [37] J. Martinek, M. Sindel, L. Borda, J. Barnaś, J. König, G. Schön, and J. von Delft, Kondo Effect in the Presence of Itinerant-Electron Ferromagnetism Studied with the Numerical Renormalization Group Method, *Phys. Rev. Lett.* **91**, 247202 (2003).
- [38] M.-S. Choi, D. Sánchez, and R. López, Kondo Effect in a Quantum Dot Coupled to Ferromagnetic Leads: A Numerical Renormalization Group Analysis, *Phys. Rev. Lett.* **92**, 056601 (2004).

- [39] A. N. Pasupathy, R. C. Bialczak, J. Martinek, J. E. Grose, L. A. K. Donev, P. L. McEuen, and D. C. Ralph, The kondo effect in the presence of ferromagnetism, *Science* **306**, 86 (2004).
- [40] J. Hauptmann, J. Paaske, and P. Lindelof, *Nat. Phys.* **4**, 373 (2008).
- [41] M. Gaass, A. K. Hüttel, K. Kang, I. Weymann, J. von Delft, and C. Strunk, Universality of the Kondo Effect in Quantum Dots with Ferromagnetic Leads, *Phys. Rev. Lett.* **107**, 176808 (2011).
- [42] J. Martinek, M. Sindel, L. Borda, J. Barnaś, R. Bulla, J. König, G. Schön, S. Maekawa, and J. von Delft, Gate-controlled spin splitting in quantum dots with ferromagnetic leads in the kondo regime, *Phys. Rev. B* **72**, 121302 (2005).
- [43] I. Weymann, Finite-temperature spintronic transport through kondo quantum dots: Numerical renormalization group study, *Phys. Rev. B* **83**, 113306 (2011).
- [44] S. Csonka, I. Weymann, and G. Zarand, An electrically controlled quantum dot based spin current injector, *Nanoscale* **4**, 3635 (2012).
- [45] D. Goldhaber-Gordon, H. Shtrikman, D. Mahalu, D. Abusch-Magder, U. Meirav, and M. A. Kastner, Kondo effect in a single-electron transistor, *Nature (London)* **391**, 156 (1998).
- [46] S. M. Cronenwett, T. H. Oosterkamp, and L. P. Kouwenhoven, A tunable kondo effect in quantum dots, *Science* **281**, 540 (1998).
- [47] R. Zitko, J. S. Lim, R. López, J. Martinek, and P. Simon, Tunable Kondo Effect in a Double Quantum Dot Coupled to Ferromagnetic Contacts, *Phys. Rev. Lett.* **108**, 166605 (2012).
- [48] K. P. Wójcik and I. Weymann, Perfect spin polarization in T-shaped double quantum dots due to the spin-dependent fano effect, *Phys. Rev. B* **90**, 115308 (2014).
- [49] L. Tosi, P. Roura-Bas, and A. A. Aligia, Transition between su(4) and su(2) kondo effect, *Physica B* **407**, 3259 (2012).
- [50] K. G. Wilson, The renormalization group: Critical phenomena and the kondo problem, *Rev. Mod. Phys.* **47**, 773 (1975).
- [51] R. Bulla, T. A. Costi, and T. Pruschke, Numerical renormalization group method for quantum impurity systems, *Rev. Mod. Phys.* **80**, 395 (2008).
- [52] K. P. Wójcik, I. Weymann, and J. Barnaś, Asymmetry-induced effects in Kondo quantum dots coupled to ferromagnetic leads, *J. Phys.: Condens. Matter* **25**, 075301 (2013).
- [53] M. Filippone, C. P. Moca, G. Zaránd, and C. Mora, Kondo temperature of su(4) symmetric quantum dots, *Phys. Rev. B* **90**, 121406 (2014).
- [54] We used the open-access Budapest Flexible DM-NRG code, <http://www.phy.bme.hu/~dmnrg/>; O. Legeza, C. P. Moca, A. I. Tóth, I. Weymann, and G. Zaránd, *arXiv:0809.3143*.
- [55] F. B. Anders and A. Schiller, Real-Time Dynamics in Quantum-Impurity Systems: A Time-Dependent Numerical Renormalization-Group Approach, *Phys. Rev. Lett.* **95**, 196801 (2005).
- [56] A. Weichselbaum and J. von Delft, Sum-Rule Conserving Spectral Functions from the Numerical Renormalization Group, *Phys. Rev. Lett.* **99**, 076402 (2007).
- [57] I. Weymann and J. Barnaś, Spin thermoelectric effects in kondo quantum dots coupled to ferromagnetic leads, *Phys. Rev. B* **88**, 085313 (2013).
- [58] R. Zitko and T. Pruschke, Energy resolution and discretization artifacts in the numerical renormalization group, *Phys. Rev. B* **79**, 085106 (2009).
- [59] Y. Meir and N. S. Wingreen, Landauer Formula for the Current through an Interacting Electron Region, *Phys. Rev. Lett.* **68**, 2512 (1992).
- [60] M. Julliere, Tunneling between ferromagnetic films, *Phys. Lett. A* **54**, 225 (1975).
- [61] J. Barnaś and I. Weymann, Spin effects in single-electron tunnelling, *J. Phys.: Condens. Matter* **20**, 423202 (2008).
- [62] L. P. Kouwenhoven, C. M. Marcus, P. L. McEuen, S. Tarucha, R. M. Westervelt, and N. S. Wingreen, Electron transport in quantum dots, in *Mesoscopic Electron Transport*, edited by L. L. Sohn, L. P. Kouwenhoven, and G. Schön (Springer Netherlands, Dordrecht, 1997), pp. 105–214.
- [63] K. P. Wójcik, Ferromagnets-induced splitting of molecular states of T-shaped double quantum dots, *Eur. Phys. J. B* **88**, 110 (2015).
- [64] I. Weymann, J. König, J. Martinek, J. Barnaś, and G. Schön, Tunnel magnetoresistance of quantum dots coupled to ferromagnetic leads in the sequential and cotunneling regimes, *Phys. Rev. B* **72**, 115334 (2005).